# Supplemental information

## Efficient rigid and flexible perovskite solar cells using strongly adsorbed molecules for lattice repair and grain boundary mitigation

Xi Fan,*[a,‡] Jiwen Chen,[a,‡] Jinzhao Wang,[b] Jing Wang,[c] Jixi Zeng,[a] Feng Wei,[a] Shuai Gao,[a] Jia Li,[a] Jing Zhang,[c] Feng Yan[d] and Weijie Song*[a,e,f]

[a]Ningbo Institute of Materials Technology and Engineering, Chinese Academy of Sciences, Ningbo, 315201, P.R. China.

[b]School of Material Science and Engineering, Hubei University, Wuhan 430062, P.R. China.

[c]School of Physical Science and Technology, Ningbo University, Ningbo 315211, P.R. China.

[d]Department of Applied Physics, The Hong Kong Polytechnic University, Hung Hom, Kowloon, Hong Kong, 999077, P. R. China.

[e]Center of Materials Science and Optoelectronics Engineering, University of Chinese Academy of Sciences, Beijing 100049, P.R. China.

[f]Research Center for Sensing Materials and Devices, Zhejiang Lab, Hangzhou, Zhejiang 311121, P.R. China.

*Correspondence: e-mail: fanxi@nimte.ac.cn; weijiesong@nimte.ac.cn

**Figure S1.** Optimized structures of perovskite (001) surface with the N1 (a), N2 (b), and N3 (c) in TD molecule, respectively. The arrow describes the bond length of Pb-N.

**DFT Calculations:**

Density functional theory (DFT) calculations were performed using the Vienna *ab initio* simulation package (VASP)[1]. Projector augmented wave (PAW) pseudopotentials[2] were used to evaluate the interactions between valence electrons and cores. The generalized gradient approximation (GGA)[3] of the Perdew-Burke-Ernzerhof (PBE) functional with DFT-D3 correction proposed by Grimme[4] was used for the exchange correlation functional. The cubic-phase $FAPbI_3$ ($\alpha$-$FAPbI_3$) was optimized for its lattice constants and atomic coordinates by using 450 eV cutoff energy and Γ-centered 6X6X6 Monkhorst-Pack (MP) mesh[5], and its convergence criteria of total energy and force were set to be less than $10^{-5}$ eV and 0.02 eV/Å, respectively. Our optimized lattice constant for $\alpha$-$FAPbI_3$ was 6.36 Å, excellent agreement with the previous theoretical and experimental value[6, 7].

To study the relationship between the additive and perovskite surfaces including (001) and (110) surfaces, and microscopic mechanism behind surface orientation regulation, we constructed 2X2 for (001) surface and 3X2 for (110) surface with the seven atomic layers to simulate the material surface. For supercell surface structures, we use a single Gamma point for the MP mesh. To avoiding the coulomb interaction between periodic surfaces, the thickness of vacuum layer was set to 15 Å. At the same time, we fixed the atoms in the two lower atomic layers to be regarded as the bulk structures, and the remaining atoms were fully relaxed to act as the perovskite surface. The adsorption energy is defined as $E_{ad}=E_{molecule@surface}-E_{molecule}-E_{surface}$. The structural visualizations were obtained by using the VESTA[8] software.

**References:**

1. Kresse, G., Furthmüller, J. Efficient iterative schemes for ab initio total-energy calculations using a plane-wave basis set. Physical review B, 54, 11169 (1996).

2. Kresse, G., Joubert, D. From ultrasoft pseudopotentials to the projector augmented-wave method, Physical review b 59, 1758 (1999).

3. Perdew, J. P., Burke, K., Ernzerhof, M. Generalized gradient approximation made simple, Physical review letters 77, 3865 (1996).

4. Grimme, S., Antony, J., Ehrlich, S., Krieg, H. A consistent and accurate ab initio parametrization of density functional dispersion correction (DFT-D) for the 94 elements H-Pu, The Journal of chemical physics 132, 154104 (2010).

5. Monkhorst, H. J., Pack, J. D. Special points for Brillouin-zone integrations, Physical review B, 13, 5188 (1976).

6. Weller, M. T., Weber, O. J., Frost J. M., Walsh, A. Cubic perovskite structure of black formamidinium lead iodide, α-$[HC(NH_2)_2]PbI_3$, at 298 K, The journal of physical chemistry letters, 6, 3209-3212 (2015).

7. Wang, J., Yin, W.-J. Effect of alloying on the carrier dynamics in high-performance perovskite solar cells, Journal of Energy Chemistry, 68, 267–274 (2022).

8. Momma K., Izumi, F. VESTA3 for three-dimensional visualization of crystal, volumetric and morphology data, 44, 1272–1276 (2011).

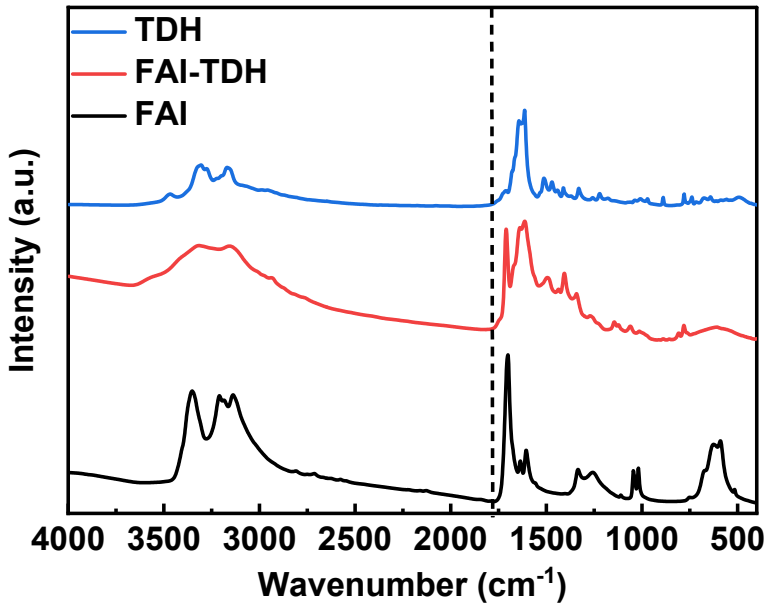


**Figure S2.** $^{1}$H NMR full spectra of TDH, FAI, and TDH and FAI complex.

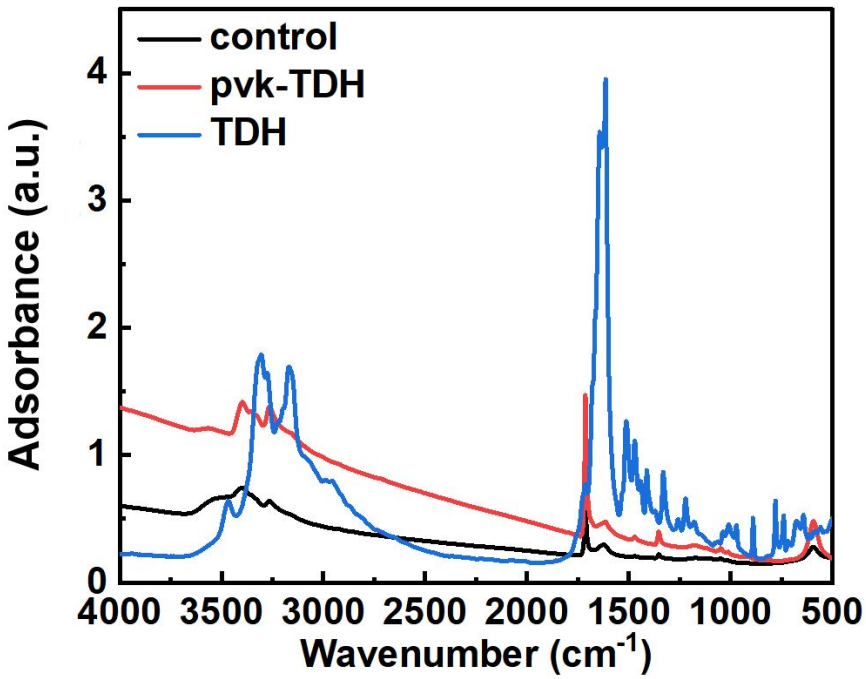


**Figure S3.** FTIR spectra of TDH, FAI (control), and TDH + FAI complex.

**Figure S4.** Topographic morphologies of the TDH perovskite films on flexible PET substrates. Scale bar: 2 µm, and 1 µm, respectively.

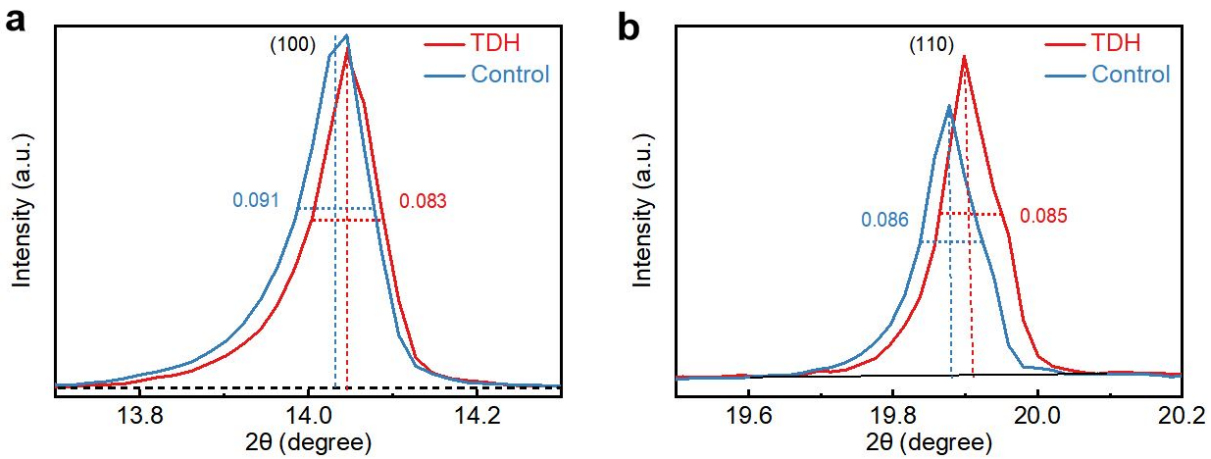


**Figure S5.** XRD spectra showing (100) (**a**) and (110) (**b**) shifts of the perovskite films with the TDH treatments.

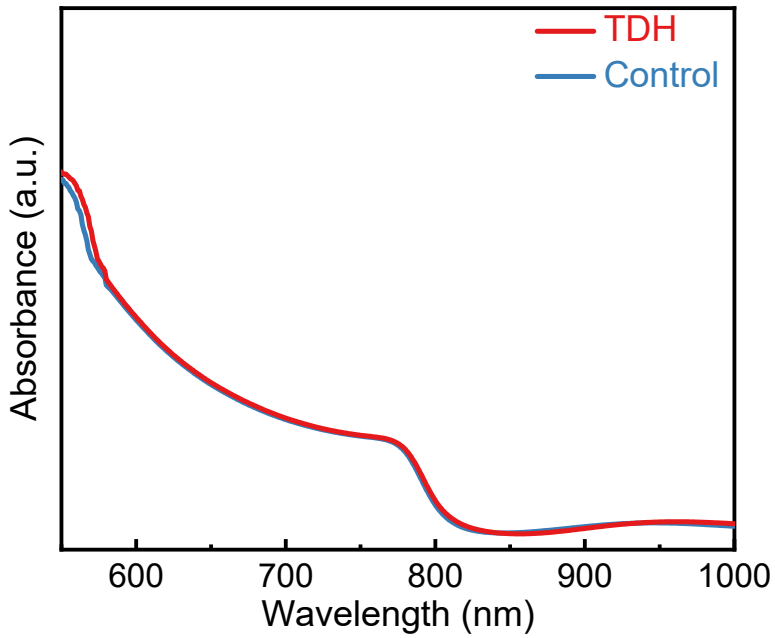


**Figure S6.** Absorption spectra of the control and TDH perovskite films.

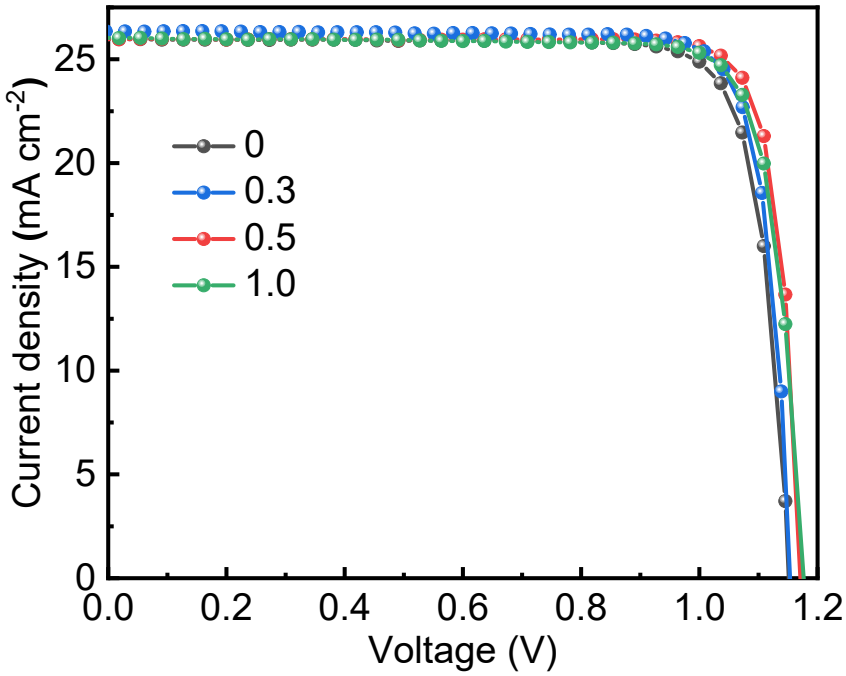


| Concentration (mg ml$^{-1}$) | $V_{OC}$ (V) | $J_{SC}$ (mA cm$^{-2}$) | FF(%) | PCE(%) |
|---|---|---|---|---|
| 0 | 1.15 | 25.96 | 83.42 | 24.93 |
| 0.3 | 1.15 | 26.34 | 84.72 | 25.64 |
| 0.5 | 1.17 | 25.99 | 85.94 | 26.15 |
| 1.0 | 1.18 | 26.02 | 83.68 | 25.61 |

**Figure S7.** The TDH concentration optimization for a better device.

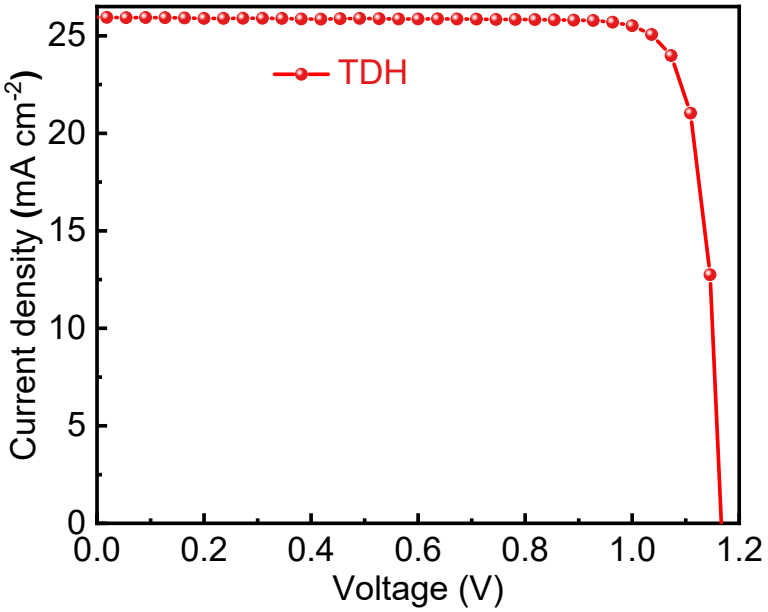


| $V_{OC}$ (V) | $J_{SC}$ (mA cm$^{-2}$) | FF (%) | PCE(%) |
|---|---|---|---|
| 1.167 | 25.94 | 86.03 | 26.03 |

**Figure S8.** *J*–*V* curve of the rigid PSCs with the TDH passivation showing the maximum FF up to 86.03%.

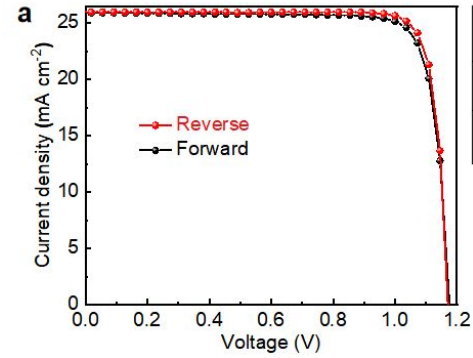


| Scaning | $V_{OC}$ (V) | $J_{SC}$ (mA cm$^{-2}$) | FF (%) | PCE (%) |
|---|---|---|---|---|
| Reverse | 1.171 | 25.99 | 85.94 | 26.15 |
| Forward | 1.176 | 25.90 | 83.65 | 25.47 |

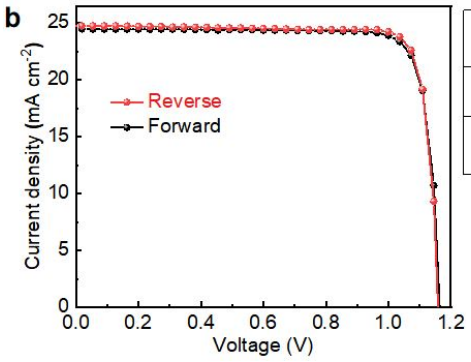


| Scaning | $V_{OC}$ (V) | $J_{SC}$ (mA cm$^{-2}$) | FF (%) | PCE (%) |
|---|---|---|---|---|
| Reverse | 1.16 | 24.74 | 86.07 | 24.68 |
| Forward | 1.16 | 24.45 | 85.17 | 24.24 |

**Figure S9.** Performance comparison of the optimized rigid (a) and flexible (b) PSCs.

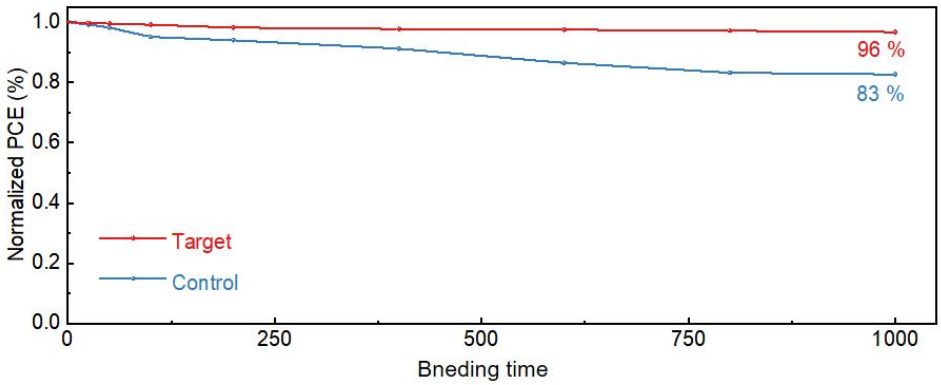


**Figure S10.** Mechanical flexibility of the flexible PSCs at a bending radius of 5.0 mm.

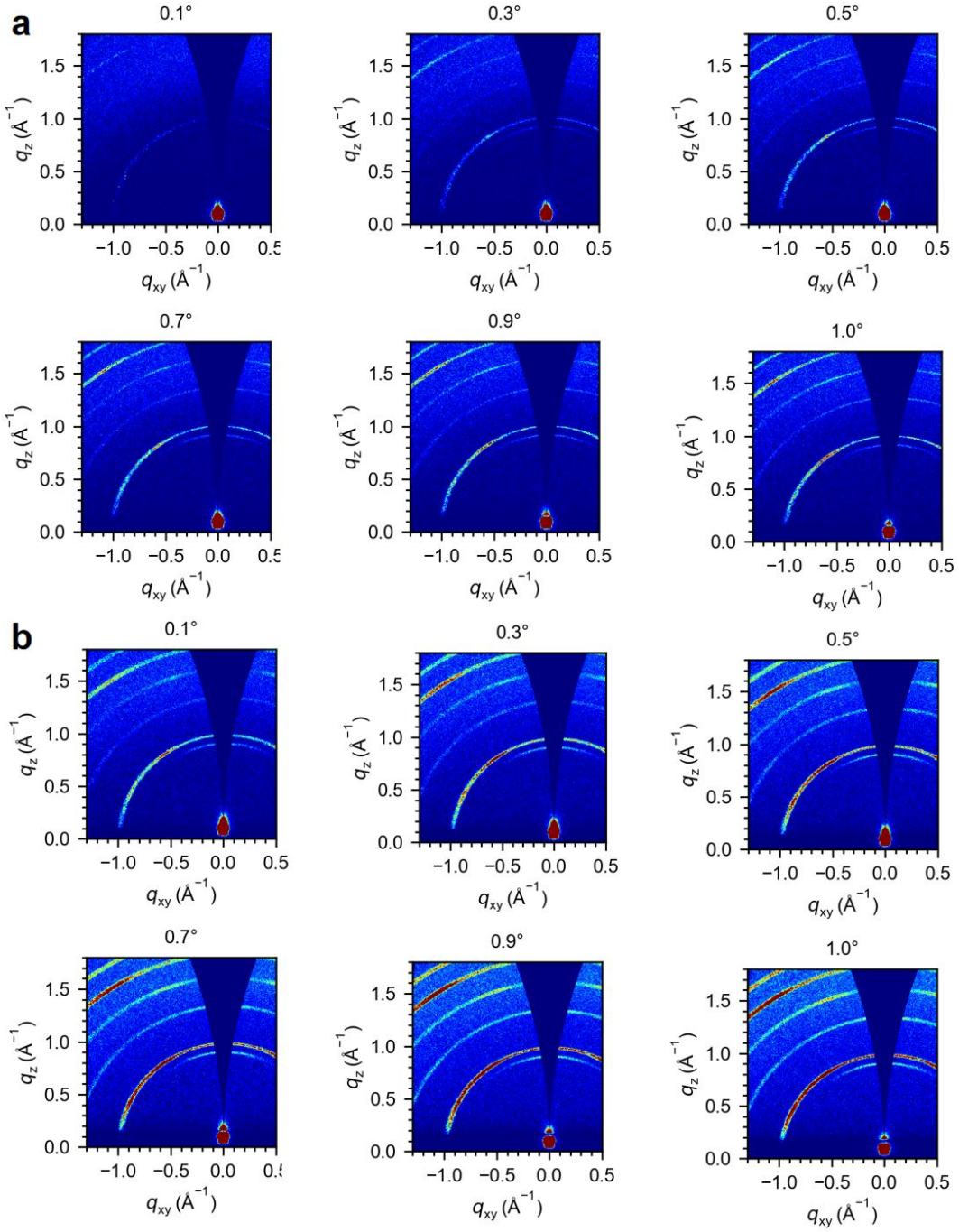


**Figure S11.** GIWAXS images of control (**a**) and TDH (**b**) perovskite films at an incidence angle of 0.1°, 0.3°, 0.5°, 0.7°, 0.9°, and 1.0°.

**Table S1.** Bond energy (eV) and Bader charge transfer (*e*) at the Pb-X (X=I and Cl) on the $FAPbI_3$ surface.

| Atoms | I | Cl |
|---|---|---|
| Bond energy (eV) | 3.24 | 4.16 |
| Bader charge transfer (*e*) | 0.19 | 0.28 |

**Table S2.** The summarized photovoltaic parameters of the champion flexible PSCs published recently.

| $V_{OC}$ [V] | $J_{SC}$ [mA cm$^{-2}$] | FF [%] | PCE [%] | Publication | Refer |
|---|---|---|---|---|---|
| 1.16 | 24.74 | 86.07 | 24.68 | Here | |
| -- | -- | 81.9 | 23.4 | Nat. Photon. 2024, 18, 379 | 1 |
| 1.19 | 25.28 | 82.1 | 24.71 | Energy Environ. Sci. 2024, 17, 2621 | 2 |
| 1.19 | 25.0 | 82.4 | 24.51 | Joule 2024, 8, 1120 | 3 |
| 1.18 | 25.14 | 80.1 | 23.70 | Energy Environ. Sci. 2024, Advance Article. doi.org/10.1039/D4EE02925A | 4 |
| 1.17 | 24.96 | 83.51 | 24.45 | Adv. Mater. 2024, 36, 2405572 | 5 |
| 1.15 | 25.49 | 83.31 | 24.48 | Adv. Mater. 2024, 36, 2403531 | 6 |
| 1.17 | 23.0 | 83.42 | 22.61 | Adv. Mater. 2024, 36, 2401236 | 7 |
| 1.16 | 24.4 | 78.2 | 22.1 | Adv. Funct. Mater. 2024, 2404686 | 8 |
| 1.14 | 25.36 | 83.57 | 24.08 | Energy Environ. Sci. 2023, 16, 5423 | 9 |
| 1.14 | 24.96 | 80.5 | 23.13 | Adv. Mater. 2023, 35, e2302752 | 10 |
| 1.17 | 24.8 | 81 | 23.68 | Adv. Mater. 2023, 35, 2206387. | 11 |
| 1.13 | 24.9 | 82 | 23.0 | Adv. Funct. Mater. 2022, 32, 2204880 | 12 |
| 1.15 | 22.55 | 80.50 | 20.90 | Adv. Funct. Mater. 2022, 32, 2205009 | 13 |
| 1.19 | 22.21 | 82.33 | 21.76 | Energy Environ. Sci. 2022, 15, 3439 | 14 |
| 1.11 | 23.50 | 80.76 | 21.08 | Adv. Mater. 2022, 34, 2201840 | 15 |
| 1.19 | 22.2 | 82.33 | 21.76 | Energy Environ. Sci. 2022, 15, 3439 | 16 |
| 1.11 | 23.50 | 80.756 | 21.08 | Adv. Mater. 2022, 34, 2201840 | 17 |
| 1.13 | 24.8 | 77.68 | 21.73 | Adv. Mater. 2021, 33, 2105539 | 18 |
| 1.07 | 23.59 | 81.22 | 20.50 | Angew. Chem. Int. Ed. 2021, 61, e202116602 | 19 |
| 1.13 | 22.05 | 81.3 | 20.27 | Adv. Funct. Mater. 2021, 31, 2103252 | 20 |

**References:**

1. Xu, W., Chen, B., Zhang, Z., Liu, Y., Xian, Y., Wang, X., Shi Z., Gu, H., Fei, C., Li, N., Uddin, M. A., Zhang, H., Dou, L., Yan, Y., Huang, J. (2024) Multifunctional entinostat enhances the mechanical robustness and efficiency of flexible perovskite solar cells and Minimodules. Nat. Photon. 18, 379–387.

2. Xue, T., Fan, B., Jiang, K., Guo, Q., Hu, X., Su, M., Zhou E., Song Y. (2024) Self-healing ion-conducting elastomer towards record efficient flexible perovskite solar cells with excellent recoverable mechanical stability. Energy Environ. Sci. 17, 2621–2630.

3. Wang, Y., Meng,Y., Liu, C., Cao, R., Han, B., Xie, L., Tian, R., Lu, X., Song, Z., Li, J., Yang, S., Lu, C., Ge, Z. Utilizing electrostatic dynamic bonds in zwitterion elastomer for self-curing of flexible perovskite solar cells, Joule 8, 1120–1141 (2024).

4. Liu, P., Wang, H., Niu, T., Yin, L., Du, Y., Lang, L., Zhang, Z., Tu, Y., Liu, X., Chen, X., Wang, S., Wu, N., Qin, R., Wang, L., Yang, S., Zhang, C., Pan, X., Liu, S., Zhao, K. Ambient scalable fabrication of high-performance flexible perovskite solar cells, Energy Environ. Sci. (2024), Advance Article. https://doi.org/10.1039/D4EE02925A.

5. Gong, C., Wang, C., Meng, X., Fan, B., Xing, Z., Shi, S., Hu, T., Huang, Z., Hu, X., Chen, Y. An Equalized Flow Velocity Strategy for Perovskite Colloidal Particles in Flexible Perovskite Solar Cells. Adv. Mater. 2405572 (2024).

6. Wu, Y., Xu, G., Shen, Y., Wu, X., Tang, X., Han, C., Chen, Y., Yang, F., Chen, H., Li, Y., Li, Y. Stereoscopic Polymer Network for Developing MechanicallyRobust Flexible Perovskite Solar Cells with an Efficiency Approaching 25%, Adv. Mater. 2403531 (2024).

7. Liu, J., Zhao, Z., Qian, J., Liang, Z., Wu, C., Wang, K., Liu, S., Yang, D. Thermal Radiation Annealing for Overcoming Processing Temperature Limitation of Flexible Perovskite Solar Cells, Adv. Mater. 36, 2401236 (2024).

8. Sun, Q., Meng, X., Liu, G., Duan, S., Hu, D., Shen, B., Kang, B., Silva, S. Ravi P. $SnO_2$ Surface Modification and Perovskite Buried Interface Passivation by 2,5-Furandicarboxylic Acid for Flexible Perovskite Solar Cells, Adv. Funct. Mater. 2404686 (2024).

9. Xie, L., Du, S., Li, J., Liu, C., Pu, Z., Tong, X., Liu, J., Wang, Y., Meng, Y., Yang, M., Li, W., Z. Ge. Molecular dipole engineering-assisted strain release for mechanically robust flexible perovskite solar cells. Energy Environ. Sci. 16, 5423–5433 (2023).

10. Xie, L., Liu. J., Li, J., Liu, C., Pu. Z., Xu. P., Wang, Y., Meng, Y., Yang, M., Ge, Z. A Deformable Additive on Defects Passivation and Phase Segregation Inhibition Enables the Efficiency of Inverted Perovskite Solar Cells over 24%, Adv. Mater. e2302752, (2023).

11. Gao, D., Li. B., Li, Z., Wu, X., Zhang, S., Zhao. D., Jiang, X., Zhang, C., Wang, Y., Li, Z., Li, N., Xiao, S., Wallace C.H., et al. Highly Efficient Flexible Perovskite Solar Cells through Pentylammonium Acetate Modification with Certified Efficiency of 23.35%. Adv. Mater. 35, 2206387 (2023).

12. Cheng, H., Liu, C., Zhuang, J., Cao, J., Wang, T., Wong, W., Yan, F. $KBF_4$ Additive for Alleviating Microstrain, Improving Crystallinity, and Passivating Defects in Inverted Perovskite Solar Cells. Adv. Funct. Mater. 32, 2204880 (2022).

13. Liu, S., Guan, X., Xiao, W., Chen, R., Zhou, J., Ren, F., Wang, J., Chen, W., Li, S., Qiu, L., Zhao, Y., Liu, Z., Chen, W. Effective Passivation with Size-Matched Alkyldiammonium Iodide for High-Performance Inverted Perovskite Solar Cells. Adv. Funct. Mater. 32, 2205009, (2022).
14. Kang, Y., Li, R., Wang, A., Kang, J.J., Wang, Z., Bi, W., Yang, Y., Song, Y., Dong, Q. Ionogel-perovskite matrix enabling highly efficient and stable flexible solar cells towards fully-R2R fabrication. Energy Environ. Sci. 15, 3439–3448 (2022).
15. Fan, B., Xiong, J., Zhang, Y., Gong, C., Li, F., Meng, X., Hu, X., Yuan, Z., Wang, F., Chen, Y. A Bionic Interface to Suppress the Coffee-Ring Effect for Reliable and Flexible Perovskite Modules with a Near-90% Yield Rate. Adv. Mater. 34, 2201840 (2022).
16. Kang, Y., Li, R., Wang, A., Kang, J. J., Wang, Z., Bi, W., Yang, Y., Song, Y., Dong, Q. Ionogel-perovskite matrix enabling highly efficient and stable flexible solar cells towards fully-R2R fabrication. Energy Environ. Sci. 15, 3439–3448 (2022).
17. Fan, B., Xiong, J., Zhang, Y., Gong, C., Li, F., Meng, X., Hu, X., Yuan, Z., Wang, F., Chen, Y. A Bionic Interface to Suppress the Coffee-Ring Effect for Reliable and Flexible Perovskite Modules with a Near-90% Yield Rate. Adv. Mater. 34, 2201840 (2022).
18. Wu, S., Li, Z., Zhang, J., Deng, X., Liu, Y., Zhou, J., Zhi, C., Yu, X., Zhu, Z., et al. Low-Bandgap Organic Bulk-Heterojunction Enabled Efficient and Flexible Perovskite Solar Cells. Adv. Mater. 33, 2105539 (2021).
19. Ge, C., Liu, X., Yang, Z., Li, H., Niu, W., Liu, X., Xong, Q. Thermal Dynamic Self-Healing Supramolecular Dopant Towards Efficient and Stable Flexible Perovskite Solar Cells. Angew. Chem. Int. Ed. 61, e202116602 (2021).
20. Li, J., Dewi, H.J., Wang, H., Zhao, J., Tiwari, N., Yantara, N., Malinauskas, T., Getautis, V., Savenije, T., Mathews, N., et al. Co-Evaporated $MAPbI_3$ with Graded Fermi Levels Enables Highly Performing, Scalable, and Flexible p-i-n Perovskite Solar Cells. Adv. Funct. Mater. 31, 2103252 (2021).

**Table S3.** q values of the (100) planes of perovskite films.

| | Grazing incidence angle (°) | q (Å$^{-1}$) |
|---|---|---|
| Control | 0.1 | 0.99268 |
| | 0.3 | 0.99260 |
| | 0.5 | 0.99062 |
| | 0.7 | 0.98981 |
| | 0.9 | 0.98923 |
| | 1.0 | 0.98915 |
| THD | 0.1 | 0.98488 |
| | 0.3 | 0.98488 |
| | 0.5 | 0.98488 |
| | 0.7 | 0.98488 |
| | 0.9 | 0.98488 |
| | 1.0 | 0.98488 |

**Table S4.** The lifetimes of the control and TDH perovskite films coated on glass substrates.

| | $A_1$ | $\tau_1$ (μs) | $A_2$ | $\tau_2$ (μs) | $\tau_a$ (μs) |
|---|---|---|---|---|---|
| Control | 13.25 | 0.13 | 0.51 | 3.59 | 1.92 |
| TDH | 0.56 | 0.66 | 0.71 | 4.27 | 3.87 |